Int. J. Heat Mass Transfer. Vol. 34, No. 4/5, pp. 899–909, 1991
Printed in Great Britain

0017-9310/91 \$3.00+0.00

Study of transient laminar free convection over an inclined wet flat plate

B. ZEGHMATI and M. DAGUENET
Laboratoire de Thermodynamique et Energétique, Université de Perpignan, Avenue de Villeneuve, 66025 Perpignan Cédex, France

and

G. LE PALEC
Institut Méditerranéen de Technologie, Technopole de Chateau-Gombert, 13451 Marseille Cédex, France

(*Received* 23 *February* 1989 *and in final form* 8 *February* 1990)

Abstract—A new analysis of the transient natural convection between an inclined wet flat plate and ambient air is presented. The problem is treated by considering two separate regions—i.e. the boundary layer and the capillary-porous plate—for which a specific differential system of equations is developed. The two systems are linked with the wall heat and mass balances from which the local and average Nusselt and Sherwood numbers are deduced. For some particular cases, quantitative comparisons with previous works reported in the literature agree with each other. Moreover, the agreement between theoretical results and experimental data is satisfactory in the boundary-layer region.

1. INTRODUCTION

BECAUSE of their applications in many physical processes, such as drying for example, the combined heat and mass transfer between capillary-porous materials and air has extensively been studied in the past 20 years. In such processes the geometry of the porous material and the nature of the surrounding flow evidently play an important part and the present study is confined to the drying of a wet inclined flat plate by free convection. This problem can be treated by considering two regions.

(1) The first is the boundary layer which grows near the surface plate. Several studies treating the boundary-layer heat and mass transfer by laminar free convection under steady-state conditions with either constant wall temperature [1–6] or constant wall heat flux [7, 8] have been published. On the other hand, a few studies about transient natural convection have been reported in the literature: note the work of Callahan and Marner [9] who studied the case of an isothermal plate. From the literature review, it appears that the numerical procedures used for solving the free convection with mass transfer problems are similar to those which were developed for heat transfer problems [10, 11]: for inclined plates, the Rich procedure [12] is generally suitable.

(2) The second region is the non-saturated capillary-porous plate for which several theories have been proposed for describing the internal heat and moisture transfer. The 'Luikov–De Vries' model [13] is nowadays commonly accepted. However, it should be noted that the equations of this model can only be integrated if the heat and mass transfer coefficients between the surface of the plate and the surrounding air are known.

The literature review shows that no study about simultaneous and transient heat and mass transfer in the porous plate and the boundary layer has been carried out. This is the purpose of the present paper in which the transient laminar boundary-layer equations are linked with the 'Luikov–De Vries' model. The linkage conditions are assured by the wall heat and mass balances.

Equations are solved with a finite difference procedure and numerical results are presented for pine wood. The results are compared with an experimental investigation of the boundary layer by means of an interferometric method.

2. THEORETICAL ANALYSIS

Consider a wet flat plate of length L and height h as shown in Fig. 1. This plate is inclined with an angle α from the vertical and is placed in ambient air, the temperature θ_∞ and vapour concentration c_∞ of which are constant. At time $t = t_0$, the upper face is subjected to a constant heat flux with density Q, so that a boundary layer grows near this surface because of buoyancy forces and induces heat and moisture gradients in the wet plate. The structure of the plate is assumed to be similar to a capillary-porous one: the internal heat and mass transfer can thus be described by means of the 'Luikov–De Vries' model.

We choose an orthogonal coordinates system, the

NOMENCLATURE

a_m	mass diffusivity of the porous material [$m^2 s^{-1}$]
a_q	thermal diffusivity of the porous material [$m^2 s^{-1}$]
c	vapour concentration in the boundary layer [$kg\ kg^{-1}$]
c^*	dimensionless vapour concentration in the boundary layer
C_p	specific heat of wet air [$J\ kg^{-1}\ K^{-1}$]
C_{pa}	specific heat of dry air [$J\ kg^{-1}\ K^{-1}$]
C_{pv}	specific heat of vapour [$J\ kg^{-1}\ K^{-1}$]
c_q^*	effective specific heat of the porous material [$J\ kg^{-1}\ K^{-1}$]
c_s	wall vapour concentration [$J\ kg^{-1}\ K^{-1}$]
D	mass diffusion coefficient of vapor in dry air [$m^2 s^{-1}$]
g	gravitational acceleration [$m\ s^{-2}$]
Gr_T^*	average modified thermal Grashof number defined by equation (21)
Gr_{cx}^*	local modified mass Grashof number defined by equation (38a)
Gr_{Tx}^*	local modified thermal Grashof number defined by equation (38b)
h	height of the porous plate [m]
h_r	relative humidity of ambient air [%]
Ko	Kossovitch number, $\varepsilon L_v w_0/(c_q^* T_p)$
K_p	thermal conductivity of the porous material [$W\ m^{-1}\ K^{-1}$]
L	length of the plate along the x-direction [m]
L_v	vaporization latent heat of water [$J\ kg^{-1}$]
Lu	Luikov number, a_m/a_q
M	moisture content (dry basis) of the porous material [$kg\ kg^{-1}$]
N^*	ratio Gr_{cx}^*/Gr_{Tx}^*
N_A	ratio Gr_c/Gr_T where Gr_c and Gr_T are defined by equations (19)
Nu_x	local Nusselt number
Nu	average Nusselt number
P	atmospheric pressure [$N\ m^{-2}$]
P_{vs}	partial pressure of saturated vapour at $y = 0$ [$N\ m^{-2}$]
Pn	Posnov number, $\delta T_p/w_0$
$q(x, t)$	local wall net heat flux per unit of area [$W\ m^{-2}$]
$q_m(x, t)$	local wall mass flux per unit of area [$W\ m^{-2}$]
Q	incident heat flux per unit of area [$W\ m^{-2}$]
Sh_x	local Sherwood number
Sh	average Sherwood number
t	time [s]
t^*	dimensionless time
t_p^*	Fourier number
T	temperature of the porous material [K]
T_p	initial temperature of the porous material [K]
T^*	dimensionless temperature of the porous material
T_s	wall temperature of the flat plate [K]
u, v	velocity components in the x- and y-directions [$m\ s^{-1}$]
u^*, v^*	dimensionless velocity components in the x^*- and y^*-directions
x, y	coordinate shown in Fig. 1
y_p	coordinates in the porous material
x^*, y^*	system of dimensionless coordinates in the boundary layers
y_p^*	dimensionless coordinates in the porous material
w	moisture content (dry basis) of the porous material [$kg\ kg^{-1}$]
w_0	initial moisture content of the porous material [$kg\ kg^{-1}$]
w^*	dimensionless moisture content of the porous material.

Greek symbols

α	sloping angle of the plate [deg]
α_{ab}	absorptance
β_c	coefficient of mass expansion with concentration
β_t	coefficient of thermal expansion with temperature [K^{-1}]
δ	thermal gradient coefficient for transfer of vapour [K^{-1}]
ε	phase conversion factor
λ	thermal conductivity of the fluid [$W\ m^{-1}\ K^{-1}$]
ν	kinematic viscosity [$m^2 s^{-1}$]
θ	fluid temperature [K]
θ^*	dimensionless temperature of the fluid
ρ	density of the fluid [$kg\ m^{-3}$]
ρ_p	density of the porous material [$kg\ m^{-3}$].

origin of which is located at point O (Fig. 1): x measures the distance from point O, along the upper face, while the normal distance is denoted by y in the boundary layer and y_p along the height of the plate. The normal distance from the y O x plane is sufficiently high and all the sides of the plate, except the upper face, are well insulated so that a two-dimensional problem can be assumed.

The linkage conditions between heat and mass transfer and the plate in the boundary layer are obtained from the thermal and mass balances at $y = 0$.

Thermal balance

$$\alpha_{ab} Q - K_p \left(\frac{\partial T}{\partial y_p}\right)_{y_p = h} - q(x, t) = 0. \quad (1)$$

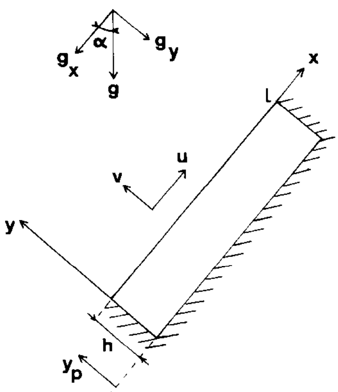

FIG. 1. Problem statement and definition of the coordinate system.

Mass balance

$$\rho_p a_m \left\{ \left(\frac{\partial w}{\partial y_p}\right)_{y_p = h} + \delta \left(\frac{\partial T}{\partial y_p}\right)_{y_p = h} \right\} = \rho D \left(\frac{\partial c}{\partial y}\right)_{y=0}. \quad (2)$$

Here T and w are respectively the temperature and the moisture content (wet basis) in the porous plate; c the vapour concentration in the boundary layer. The net wall heat flux $q(x, t)$ may be written as

$$q(x,t) = q_w(x,t) - (1-\varepsilon) L_v q_m(x,t) \quad (3)$$

where the radiative emissivity of the plate has been neglected. $q_w(x, t)$ and $(1-\varepsilon)L_v q_m(x, t)$ are the sensible heat flux and the latent heat flux, respectively. The other symbols appearing in equations (1) and (2) are defined in the Nomenclature.

As explained above, the problem may be divided into two regions—the boundary layer and the porous plate. Upon assuming the Boussinesq and Rich approximations and negligible dissipative effects, the boundary-layer equations can be given as follows (system I).

Continuity

$$\frac{\partial \rho}{\partial t} + \rho \left(\frac{\partial u}{\partial x} + \frac{\partial v}{\partial y}\right) = 0. \quad (4)$$

Momentum

$$\frac{\partial u}{\partial t} + u\frac{\partial u}{\partial x} + v\frac{\partial u}{\partial y} = v\frac{\partial^2 u}{\partial y^2} + g\cos(\alpha)[\beta_t(\theta - \theta_\infty) + \beta_c(c - c_\infty)]. \quad (5)$$

Energy

$$\frac{\partial \theta}{\partial t} + u\frac{\partial \theta}{\partial x} + v\frac{\partial \theta}{\partial y} = \frac{\lambda}{\rho C_p}\frac{\partial^2 \theta}{\partial y^2} + D\frac{C_{pv} - C_{pa}}{C_p}\frac{\partial \theta}{\partial y}\frac{\partial c}{\partial y}. \quad (6)$$

Mass

$$\frac{\partial c}{\partial t} + u\frac{\partial c}{\partial x} + v\frac{\partial c}{\partial y} = D\frac{\partial^2 c}{\partial y^2} \quad (7)$$

where u and v are the velocity components along the x- and y-directions, respectively; θ the temperature of air in the boundary layer and ρ the density of air. The other symbols are defined in the Nomenclature.

For the porous plate, we have the following equations (system II).

Energy

$$\frac{\partial T}{\partial t} = a_q \left[\frac{\partial^2 T}{\partial x^2} + \frac{\partial^2 T}{\partial y_p^2}\right] + \frac{\varepsilon L}{c_q^*}\frac{\partial w}{\partial t}. \quad (8)$$

Mass

$$\frac{\partial w}{\partial t} = a_m \left\{\frac{\partial^2 w}{\partial x^2} + \frac{\partial^2 w}{\partial y_p^2} + \delta\left[\frac{\partial^2 T}{\partial x^2} + \frac{\partial^2 T}{\partial y_p^2}\right]\right\}. \quad (9)$$

The initial and boundary conditions are given as follows.

For $t < t_0$:

$$\left.\begin{aligned} u(x,y,t) &= 0 \\ v(x,y,t) &= 0 \\ \theta(x,y,t) &= \theta_\infty \\ c(x,y,t) &= c_\infty \\ T(x,y_p,t) &= \theta_\infty \\ w(x,y_p,t) &= w_0 \\ q_w(x,t) &= q_m(x,t) = 0. \end{aligned}\right\} \quad (10)$$

For $y = 0$: $c(x, 0, t) = c_s$ where c_s is defined as a function of θ according to equation (15).

For $t \geqslant t_0$:

System I

For $y = 0$:

$$\left.\begin{aligned} u(x,0,t) &= 0 \\ v(x,0,t) &= -\frac{D}{c_s}\left(\frac{\partial c}{\partial y}\right)_{y=0} \\ q(x,t) &= -\lambda\left(\frac{\partial \theta}{\partial y}\right)_{y=0} - (1-\varepsilon)L_v D\rho\left(\frac{\partial c}{\partial y}\right)_{y=0}. \end{aligned}\right\} \quad (11)$$

For $y \to \infty$:

$$\left.\begin{aligned} u(x,y,t) &\to 0 \\ v(x,y,t) &\to 0 \\ \theta(x,y,t) &\to \theta_\infty \\ c(x,y,t) &\to c_\infty. \end{aligned}\right\} \quad (12)$$

System II

For $y_p = 0$ and $0 < x < L$:

$$\left(\frac{\partial T}{\partial y_p}\right)_{y_p=0} = 0; \quad \left(\frac{\partial w}{\partial y_p}\right)_{y_p=0} = 0. \quad (13)$$

For $0 < y_p < h$:

$$\left.\begin{aligned} \left(\frac{\partial T}{\partial x}\right)_{x=L} &= \left(\frac{\partial T}{\partial x}\right)_{x=0} = 0 \\ \left(\frac{\partial w}{\partial x}\right)_{x=L} &= \left(\frac{\partial w}{\partial x}\right)_{x=0} = 0. \end{aligned}\right\} \quad (14)$$

For $y_p = h$ and $0 < x < L$, the boundary conditions of system II are given by the thermal and mass balances (1) and (2).

In equations (11), c_s is the wall vapour concentration of air: it can be expressed from

$$c_s = 0.622\frac{h_r P_{vs}}{P - 0.378 h_r P_{vs}} \tag{15}$$

where P is the atmospheric pressure whereas P_{vs} and h_r respectively denote the partial pressure of saturated vapour at the wall temperature T_s and the relative humidity of air. P_{vs} is given by the Bertrand formula [14]

$$P_{vs}(T_s) = 10^{22.443 - 2795/T_s - 3.868\log_{10} T_s} \tag{16}$$

and it is assumed that the wall equilibrium moisture content M (dry basis) for a given relative humidity of air is represented by the Bradley model [15]

$$h_r = \exp\left(-K_2 - K_1^{100M - K_3}\right) \tag{17}$$

where K_1, K_2 and K_3 depend on the structure of the porous plate. For wood [16]

$$\left.\begin{aligned} K_1 &= 0.501 + 0.00262 T_s - 0.505\times 10^{-5} T_s^2 \\ K_2 &= -7.63 + 0.807 T_s - 0.144\times 10^{-5} T_s^2 \\ K_3 &= 0.0144 + 0.295\times 10^{-4} T_s. \end{aligned}\right\} \tag{18}$$

Equations (4)–(8) and boundary conditions (10)–(14) have been transformed by introducing the following dimensionless variables and functions.

For system I

$$x^* = \frac{x}{L},\quad y^* = \frac{y}{L} Gr_L^{*1/5},\quad t^* = \frac{\nu t}{L^2} Gr_L^{*2/5},$$

$$u^* = \frac{uL}{\nu} Gr_L^{*-2/5},\quad v^* = \frac{vL}{\nu} Gr_L^{*-2/5},$$

$$\theta^* = \frac{g\beta_t(\theta - \theta_\infty)L^3}{\nu^2}\cos(\alpha) Gr_L^{*-4/5} = Gr_T\, Gr_L^{*-4/5},$$

$$c^* = \frac{g\beta_c(c - c_\infty)L^3}{\nu^2}\cos(\alpha) Gr_L^{*-4/5} = Gr_c\, Gr_L^{*-4/5}. \tag{19}$$

For system II

$$\left.\begin{aligned} y_p^* &= \frac{y_p}{h}, & t_p^* &= \frac{t a_q}{h^2} \\ T^* &= \frac{T}{\theta_\infty}, & w^* &= \frac{w}{w_0} \end{aligned}\right\} \tag{20}$$

where

$$Gr_L^* = \frac{g\beta_t q(x,t)\cos(\alpha) L^4}{\lambda \nu^2}. \tag{21}$$

Substituting equations (19)–(21) into differential systems I and II, we obtain the following.

For system I

$$\frac{\partial u^*}{\partial x^*} + \frac{\partial v^*}{\partial y^*} = 0 \tag{22}$$

$$\frac{\partial u^*}{\partial t^*} + u^*\frac{\partial u^*}{\partial x^*} + v^*\frac{\partial u^*}{\partial y^*} = \frac{\partial^2 u^*}{\partial y^{*2}} + \theta^* + c^* \tag{23}$$

$$\frac{\partial \theta^*}{\partial t^*} + u^*\frac{\partial \theta^*}{\partial x^*} + v^*\frac{\partial \theta^*}{\partial y^*} = \frac{1}{Pr}\frac{\partial^2\theta^*}{\partial y^{*2}} + EH\frac{C_{pv} - C_{pa}}{C_p}\frac{1}{Sc}\frac{\partial\theta^*}{\partial y^*}\frac{\partial c^*}{\partial y^*} \tag{24}$$

$$\frac{\partial c^*}{\partial t^*} + u^*\frac{\partial c^*}{\partial x^*} + v^*\frac{\partial c^*}{\partial y^*} = \frac{1}{Sc}\frac{\partial^2 c^*}{\partial y^{*2}}. \tag{25}$$

In the energy equation, the dimensionless parameter EH is defined as

$$EH = \frac{q(x,t)\beta_t}{\lambda\beta_c} Gr_L^{*-1/5} \tag{26}$$

whereas Pr and Sc are the Prandtl and Schmidt numbers.

For system II

$$\frac{\partial T^*}{\partial t_p^*} = \left(\frac{h}{L}\right)^2\frac{\partial^2 T^*}{\partial x^{*2}} + \frac{\partial^2 T^*}{\partial y_p^{*2}} + \varepsilon\, Ko\frac{\partial w^*}{\partial t_p^*} \tag{27}$$

$$\frac{\partial w^*}{\partial t_p^*} = Lu\left\{\left(\frac{h}{L}\right)^2\frac{\partial^2 w^*}{\partial x^{*2}} + \frac{\partial^2 w^*}{\partial y_p^{*2}} + Pn\left[\left(\frac{h}{L}\right)^2\frac{\partial^2 T^*}{\partial x^{*2}} + \frac{\partial^2 T^*}{\partial y_p^{*2}}\right]\right\} \tag{28}$$

where Ko, Lu and Pn are respectively the Kossovitch, Luikov and Posnov numbers, the definitions of which are given in the Nomenclature. The initial and boundary conditions (10)–(14) are given as follows.

For $t^* < t_0^*$:

$$u^*(x^*,y^*,t^*) = v^*(x^*,y^*,t^*) = \theta^*(x^*,y^*,t^*) = c^*(x^*,y^*,t^*) = 0$$

$$T^*(x^*,y_p^*,t_p^*) = w^*(x^*,y_p^*,t_p^*) = 1. \tag{29}$$

For $t^* \geq t_0^*$:
System I

$$\left.\begin{aligned} & u^*(x^*,y^*,t^*) = 0 \\ & v^*(x^*,y^*,t^*) = -\frac{Dxq(x,t)\beta_t\, Gr_L^{*-1/5}}{\lambda\nu\beta_c(1-c_s)}\left(\frac{\partial c^*}{\partial y^*}\right)_{y^*=0} \\ & \left(\frac{\partial\theta^*}{\partial y^*}\right)_{y^*=0} + (1-\varepsilon)\frac{LD\rho\beta_t}{\lambda\beta_c}\left(\frac{\partial c^*}{\partial y^*}\right)_{y^*=0} = -1 \\ & c_s^* = \frac{g\beta_c(c_s - c_\infty)l^3}{\nu^2} Gr^{*-1.5}. \end{aligned}\right\} \tag{30}$$

For $y^* \to \infty$:

$$\left.\begin{aligned} u^*(x^*,y^*,t^*) &\to 0 \\ v^*(x^*,y^*,t^*) &\to 0 \\ \theta^*(x^*,y^*,t^*) &\to 0 \\ c^*(x^*,y^*,t^*) &\to 0. \end{aligned}\right\} \tag{31}$$

System II

For $y_p^* = 0$ and $0 < x^* < 1$:

$$\left(\frac{\partial T^*}{\partial y_p^*}\right)_{y_p^*=0} = \left(\frac{\partial w^*}{\partial y_p^*}\right)_{y_p^*=0} = 0. \quad (32)$$

For $0 < y_p^* < 1$

$$\left(\frac{\partial T^*}{\partial x^*}\right)_{x^*=0} = \left(\frac{\partial T^*}{\partial x^*}\right)_{x^*=1} = \left(\frac{\partial w^*}{\partial x^*}\right)_{x^*=0} = \left(\frac{\partial w^*}{\partial x^*}\right)_{x^*=1} = 0. \quad (33)$$

Finally, the dimensionless form of the linkage conditions (1) and (2) are given as follows.

For thermal balance

$$\frac{K_p\theta_\infty}{\alpha_{ab}Qh}\left(\frac{\partial T^*}{\partial y_p^*}\right)_{y_p^*=1} - \frac{q(x,t)}{\alpha_{ab}Q}\left(\frac{\partial \theta^*}{\partial y^*}\right)_{y^*=0} - \frac{(1-\varepsilon)L_vDq(x,t)\rho\beta_t}{\lambda\beta_c\alpha_{ab}Q}\left(\frac{\partial c^*}{\partial y^*}\right)_{y^*=0} = 1. \quad (34)$$

For mass balance

$$\left(\frac{\partial w^*}{\partial y_p^*}\right)_{y_p^*=1} + \frac{\delta\theta_\infty}{w_0}\left(\frac{\partial T^*}{\partial y_p^*}\right)_{y_p^*=1} = \frac{hDq(x,t)\rho\beta_t}{\rho_p a_m \beta_m \lambda w_0}\left(\frac{\partial c^*}{\partial y^*}\right)_{y^*=0}. \quad (35)$$

From the dimensionless temperature and vapour concentration defined by equations (19) and the definition of the heat and mass transfer coefficients, it can be shown that the local Nusselt and Sherwood numbers are

$$\left.\begin{aligned} Nu_x &= -\frac{x^*\,Gr_L^{*\,1/5}\left(\frac{\partial \theta^*}{\partial y^*}\right)_{y^*=0}}{\theta^*(x^*,0,t^*)} \\ Sh_x &= -\frac{x^*\,Gr_L^{*\,1/5}\left(\frac{\partial c^*}{\partial y^*}\right)_{y^*=0}}{c^*(x^*,0,t^*)}. \end{aligned}\right\} \quad (36)$$

From the above we can define the ratio Sh_x/Nu_x

$$\frac{Sh_x}{Nu_x} = \frac{1}{N_A}\frac{Gr_{cx}^*}{Gr_{Tx}^*} = \frac{N^*}{N_A} \quad (37)$$

with

$$Gr_{cx}^* = \frac{q_m(x,t)\beta_c x}{\rho D} \quad (38a)$$

$$Gr_{Tx}^* = \frac{q_w(x,t)\beta_t x}{\lambda} \quad (38b)$$

$$N_A = \frac{\beta_c(c_s - c_\infty)}{\beta_t(T_s - \theta_\infty)}. \quad (38c)$$

The ratio N^* compares the thermal diffusion with the mass diffusion. The buoyancy thermal force opposes the buoyancy mass forces when N^* or N_A is negative and aids it for positive values of N^* or N_A. The average Nusselt and Sherwood numbers are obtained by integrating equations (36) over the plate surface

$$\left.\begin{aligned} \overline{Nu} &= \int_0^1 Nu_x\,dx^* \\ \overline{Sh} &= \int_0^1 Sh_x\,dx^*. \end{aligned}\right\} \quad (39)$$

3. NUMERICAL PROCEDURE

The differential equations (22)–(28) together with initial and boundary conditions (29)–(33) and linkage dimensionless balances (34) and (35) have been discretized by means of an implicit finite difference scheme. The resulting algebraic system has been treated with the factorization method [17] for the boundary layer whereas the iterative Gauss–Seidel procedure has been used for the 'Luikov' equations [18].

At time t^* and for a given abscissa x^*, the boundary-layer equations were solved over the range $0 \leqslant y^* \leqslant \delta^*(x^*)$, where $\delta^*(x^*)$ is the dimensionless boundary-layer thickness which has been defined, as usual, by assuming that

$$F = \max\{u^*, v^*, \theta^*, c^*\} < 10^{-2}. \quad (40)$$

Equations were then solved for $x^* + \Delta x^*$ and so on until the abscissa $x^* = 1$ was reached. For the treatment of the Luikov equations, the wall dimensionless temperature and vapour concentration derivatives were approached with a five-point interpolation formula. The dimensionless temperature and moisture content distributions of the porous plate were then calculated before computing the wall heat and mass fluxes defined in equations (1) and (2). Once the convergence has been reached, the average Nusselt and Sherwood numbers were computed using Simpson's integral method.

The above procedure was repeated for $t^* + \Delta t^*$, where Δt^* is the dimensionless time step, until the steady-state regime was reached. This state has been defined by assuming a 10^{-4} departure for the local Nusselt and Sherwood number between times t^* and $t^* + \Delta t^*$. The numerical procedure could then either be stopped or continued until a fixed mean value of the moisture content was obtained.

4. RESULTS AND DISCUSSIONS

For some particular cases, the numerical procedure was first validated by comparing our results with the previously published ones in the bulk of the heat and mass boundary-layer problems. To our knowledge, Callahan and Marner [9] are the authors who gave results for the transient natural convection over an isothermal flat plate and our average Nusselt and

Table 1. Comparison between our results and equations (41) for the steady free convection over an isothermal flat plate

	Ref. [19]		This study	
Gr_x	Nu_x	Sh_x	Nu_x	Sh_x
2.01E7	24.457	23.247	25.245	24.028
4.401E7	29.405	27.644	30.151	28.123
6.264E7	31.766	30.195	31.886	31.856
7.347E7	33.060	31.423	34.133	32.080

Sherwood numbers then agree with a less than 2% departure. For the steady-state regime, the calculated values of Nu_x and Sh_x were compared with the following relationships [19]:

$$\left.\begin{aligned} Nu_x &= 0.5105\left(\frac{Gr_x}{4}\right)^{1/4} \\ Sh_x &= 0.4806\left(\frac{Gr_x}{4}\right)^{1/4} \end{aligned}\right\} \tag{41}$$

where

$$Gr_x = \frac{g\beta_t(T_s-\theta_\infty)x^3}{\nu^2}.$$

For the vertical plate particular case, Figs. 2–4, respectively, show the dimensionless u^* velocity component, concentration and temperature profiles as functions of the y^* coordinate and time t. During the transient state, the thermal boundary-layer thickness is time increasing, because of the heating of the plate, whereas the mass and hydrodynamic ones decrease.

At the very beginning of the drying process ($t < 60$ s), the temperature of the surface is constant because of the thermal inertia of the porous plate and the wall moisture content also stays constant as long as the temperature difference between the wall and ambient air is. During this stage, heat and concentration wall gradients are driven by conduction and diffusion because the boundary layer is not fully developed. Once the buoyancy forces have induced a boundary-layer flow type, heat and moisture are removed by convection which becomes the main transport mechanism as compared with conduction and diffusion. The average wall temperature is then time increasing but the average Nusselt number first decreases a lot because the thermal boundary-layer thickness grows up and the wall latent heat flux diminishes as the

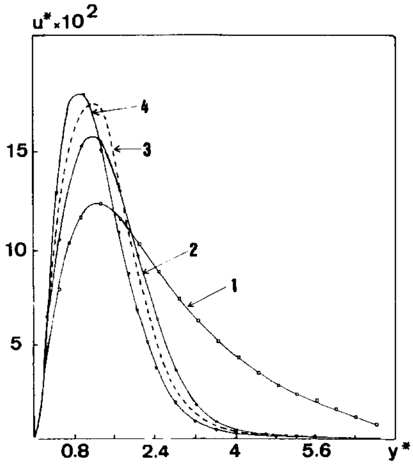

FIG. 2. Velocity profile in the boundary layer at $x^* = 1$. 1, $t = 10$ s; 2, $t = 1$ h; 3, $t = 10$ h; 4, $t = 14$ h; $w_0 = 5$ kg kg^{-1} (dry basis); $\varepsilon = 0.5$; $\theta_\infty = 25°$C; $h_r = 5\%$; $Q = 500$ W m^{-2}; $\alpha = 40°$.

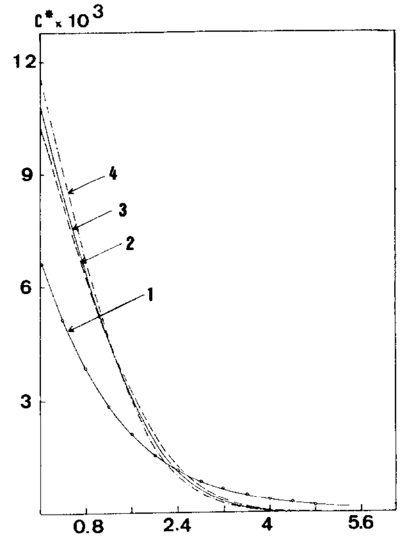

FIG. 3. Concentration profile in the boundary layer at $x^* = 1$. 1, $t = 10$ s; 2, $t = 1$ h; 3, $t = 10$ h; 4, $t = 14$ h; $w_0 = 5$ kg kg^{-1} (dry basis); $\varepsilon = 0.5$; $\theta_\infty = 25°$C; $h_r = 5\%$; $Q = 500$ W m^{-2}; $\alpha = 40°$.

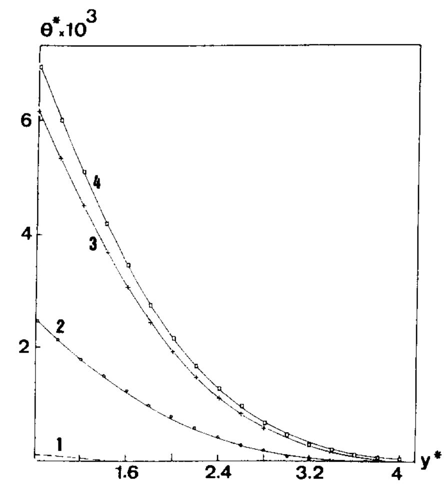

FIG. 4. Temperature profile in the boundary layer at $x^* = 1$. 1, $t = 10$ s; 2, $t = 1$ h; 3, $t = 10$ h; 4, $t = 14$ h; $w_0 = 5$ kg kg^{-1} (dry basis); $\varepsilon = 0.5$; $\theta_\infty = 25°$C; $h_r = 5\%$; $Q = 500$ W m^{-2}; $\alpha = 40°$.

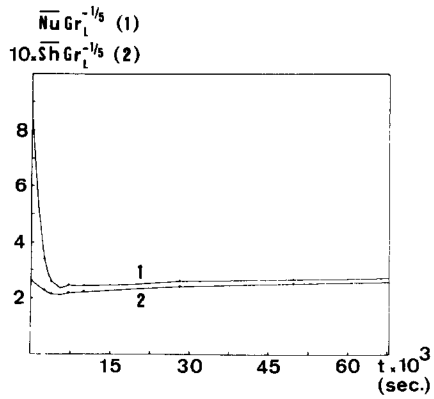

FIG. 5. Variations of the average Nusselt (curve 1) and Sherwood (curve 2) numbers during the transient state at $x^* = 1$: $w_0 = 5$ kg kg^{-1} (dry basis); $\varepsilon = 0.5$; $\theta_\infty = 25°C$; $h_r = 5\%$; $Q = 500$ W m^{-2}; $\alpha = 0°$.

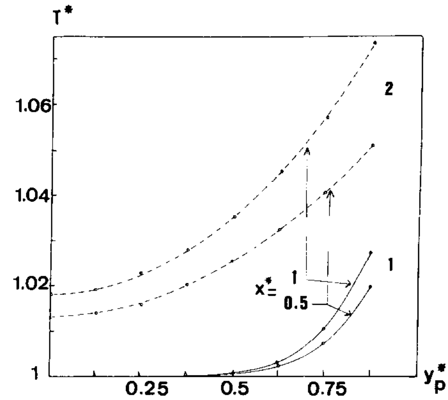

FIG. 7. Temperature distributions in the porous plate. For $x^* = 0.5$ and 1. 1, $t = 1$ h; 2, $t = 14$ h; $w_0 = 5$ kg kg^{-1} (dry basis); $\varepsilon = 0.5$; $\theta_\infty = 25°C$; $h_r = 5\%$; $Q = 500$ W m^{-2}; $\alpha = 0°$.

surface is dried (Fig. 5). This drying also acts on the value of the average Sherwood number. Both $\overline{Nu}$ and $\overline{Sh}$ are a minimum for approximately $t = 5000$ s and then slowly increase as long as internal moisture can be removed from the porous material. The corresponding local values of the Nusselt and Sherwood numbers are plotted in Fig. 6 for $t = 1$, 6 and 14 h: these curves show that the temperature and concentration differences between the wall and ambient air are lower at the bottom of the plate, where evaporative cooling accompanying the wall moisture evaporation is minimal.

The dimensionless temperature and moisture content profiles in the porous plate are respectively reported on Figs. 7 and 8 for $x^* = 0.5$ and 1 at $t = 1$ and 14 h. Under the effect of the constant wall heating flux Q, the temperatures of all locations in the plate increase with time and are higher from the bottom to the top, as explained above. The moisture content is seen to decrease with time and is highly correlated with the position of the thermal vaporization zone which is deeper as time increases. It should be noted that the moisture removed also depends on the vapour diffusion from the evaporation zone to the surface of the plate, which means that the physical structure of the porous material acts on heat and mass transfer in the boundary layer. This phenomenon can be visualized by varying the value of the vaporization factor ε, as shown in Fig. 9.

In Fig. 10, the local Nusselt and Sherwood numbers are plotted against the x^* coordinate for three values of the inclination angle $\alpha = 0°$ (vertical plate), 30° and 60°. These values were obtained at a time of 120 s, when the thermal, mass and hydrodynamic boundary layers are fully developed. As α is higher, the active component of buoyancy forces, which generate the free convection, proportionally decreases with cos (α), inducing smaller local heat and mass transfer co-

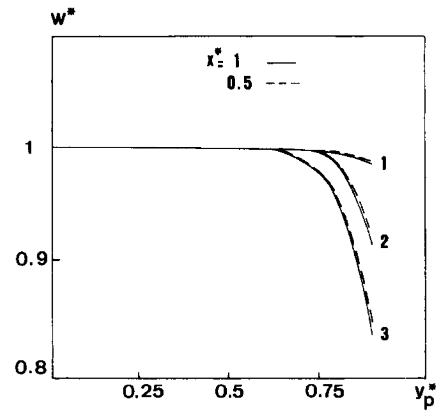

FIG. 8. Moisture content distributions in the porous plate for $x^* = 1$ and 0.5. 1, $t = 1$ h; 2, $t = 3$ h; 3, $t = 14$ h; $w_0 = 5$ kg kg^{-1} (dry basis); $\varepsilon = 0.5$; $\theta_\infty = 25°C$; $h_r = 5\%$; $Q = 500$ W m^{-2}; $\alpha = 0°$; $\theta_i = 25°C$.

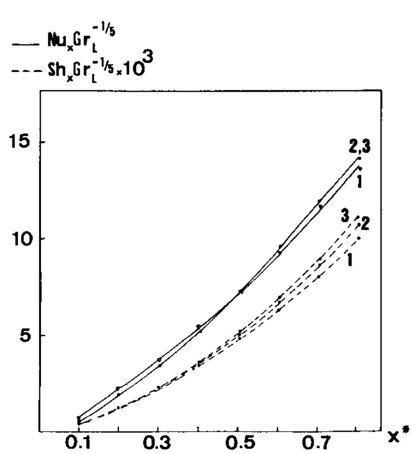

FIG. 6. Variations of the local Nusselt (a) and Sherwood (b) numbers at $x^* = 1$: 1, $t = 1$ h; 2, $t = 6$ h; 3, $t = 14$ h; $w_0 = 5$ kg kg^{-1} (dry basis); $\varepsilon = 0.5$; $\theta_\infty = 25°C$; $h_r = 5\%$; $Q = 500$ W m^{-2}; $\alpha = 0°$.

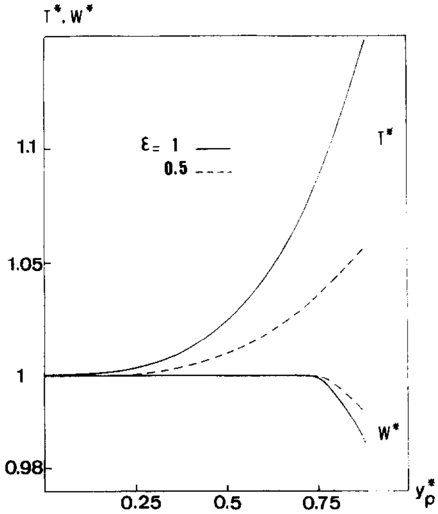

FIG. 9. Effect of the phase conversion factor ε on temperature and moisture content distributions in the porous plate at $x^* = 1$. 1, $\varepsilon = 0.5$; 2, $\varepsilon = 1$; $t = 3$ h; $w_0 = 5$ kg kg^{-1} (dry basis); $\theta_\infty = 25°$C; $h_r = 5\%$; $Q = 500$ W m^{-2}; $\alpha = 0°$.

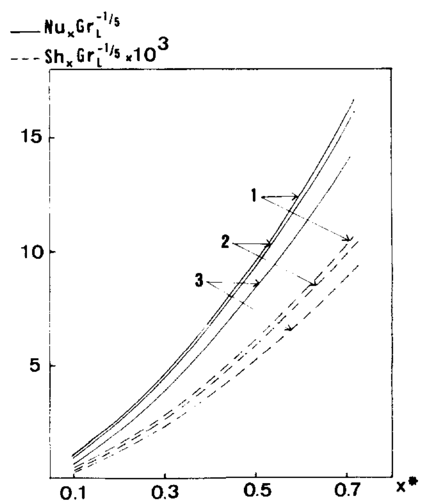

FIG. 10. Variations of the local Nusselt and Sherwood numbers with the inclination angle of the plate at $x^* = 1$. 1, $\alpha = 0°$ (vertical plate); 2, $\alpha = 30°$; 3, $\alpha = 60°$; $t = 120$ s; $w_0 = 5$ kg kg^{-1} (dry basis); $\varepsilon = 0.5$; $\theta_\infty = 25°$C; $h_r = 5\%$; $Q = 500$ W m^{-2}.

efficients. It follows that the moisture removed from the plate also decreases as α is higher. The corresponding dimensionless u^* velocity component, temperature and concentration profiles in the boundary layer are shown in Figs. 11–13: it is noted that the wall temperature and concentration decreases whereas the mass and thermal boundary-layers thicknesses increase as α is higher, which explains the results given in Fig. 10. All other comments which have been outlined for the vertical plate case are also valid for the inclined plate one.

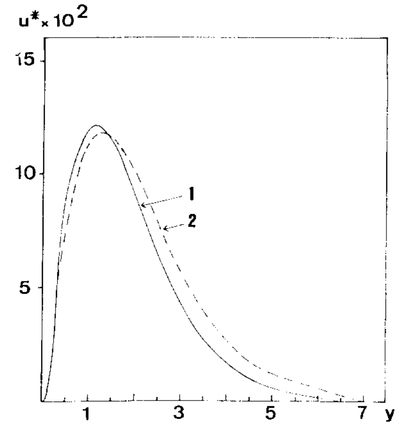

FIG. 11. Velocity profile in the boundary layer as a function of the inclination angle of the plate at $x^* = 1$. $t = 120$ s; 1, $\alpha = 30°$; 2, $\alpha = 60°$; $\varepsilon = 0.5$; $w_0 = 5$ kg kg^{-1} (dry basis); $\theta_\infty = 25°$C; $h_r = 5\%$; $Q = 500$ W m^{-2}.

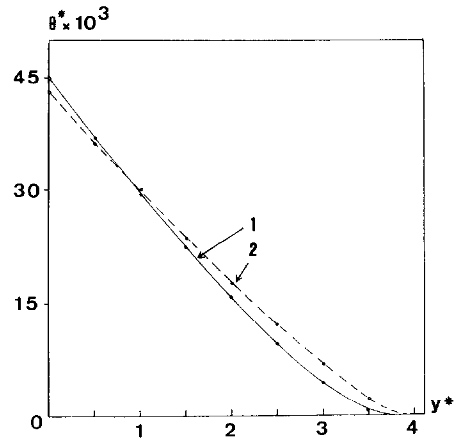

FIG. 12. Temperature profile in the boundary layer as a function of the inclination angle of the plate at $x^* = 1$. 1, $\alpha = 30°$; 2, $\alpha = 60°$; $\varepsilon = 0.5$; $t = 120$ s; $w_0 = 5$ kg kg^{-1} (dry basis); $\theta_\infty = 25°$C; $h_r = 5\%$; $Q = 500$ W m^{-2}.

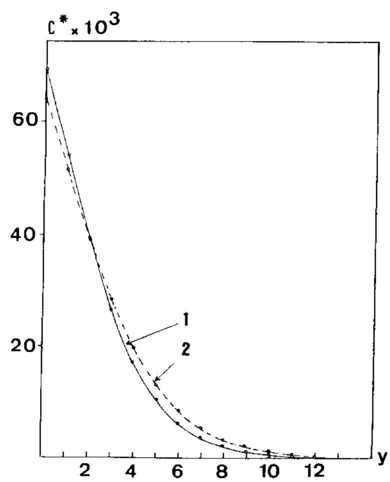

FIG. 13. Concentration profile in the boundary layer as a function of the inclination angle of the plate at $x^* = 1$. 1, $\alpha = 30°$; 2, $\alpha = 60°$; $\varepsilon = 0.5$; 1, $t = 120$ s; $w_0 = 5$ kg kg^{-1} (dry basis); $\theta_\infty = 25°$C; $h_r = 5\%$; $Q = 500$ W m^{-2}.

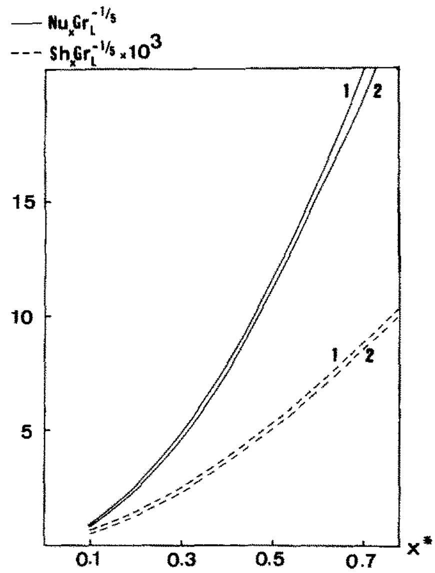

FIG. 14. Effect of the vapour velocity at the wall on the local Nusselt and Sherwood numbers at $x^* = 1$. 1, velocity is given by boundary conditions (11); 2, $v = 0$ for $y = 0$; $\alpha = 60°$; $\varepsilon = 0.5$; $t = 60$ s; $w_0 = 5$ kg kg^{-1} (dry basis); $\theta_\infty = 25°$C; $h_r = 5\%$; $Q = 500$ W m^{-2}.

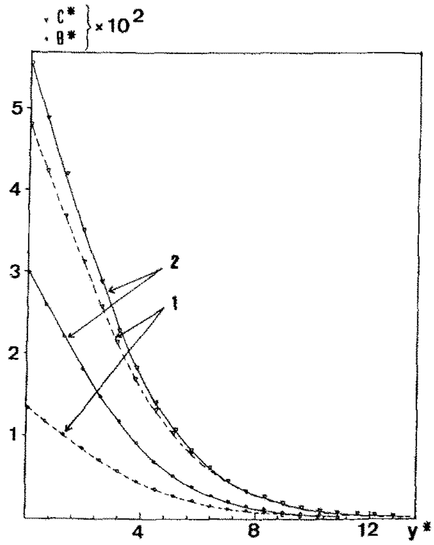

FIG. 15. Effect of the sensible heat of the removed vapour on dimensionless temperature and concentration profiles in the boundary layer at $x^* = 1$. 1, sensible heat is neglected in the calculations; 2, sensible heat is not neglected. $t = 120$ s; $\varepsilon = 0.5$; $x^* = 1$; $w_0 = 5$ kg kg^{-1} (dry basis); $\theta_\infty = 25°$C; $h_r = 5\%$; $Q = 800$ W m^{-2}.

In order to illustrate the effect of the vapour velocity at the wall, the value of which being calculated from boundary conditions (11), the local Nusselt and Sherwood numbers have been compared with those resulting from the usual assumption, that is $v = 0$ for $y = 0$. Figure 14 shows that this assumption is practically justified. On the other hand, it should be noted that the sensible heat of the removed vapour modifies the dimensionless temperature and concentration profiles in the boundary layer, as shown in Fig. 15 for $x^* = 1$ and $\alpha = 0°$.

Finally it appears from Fig. 16 that an increase of either the incident wall heat flux Q or the initial moisture content w_0 leads to a better heat and mass transfer from the plate. This figure presents the variations of the ratio N^* as a function of the x^* coordinate: recalling the definition of N^*, it thus illustrates the comparison between the intensities of thermal and mass buoyancy forces.

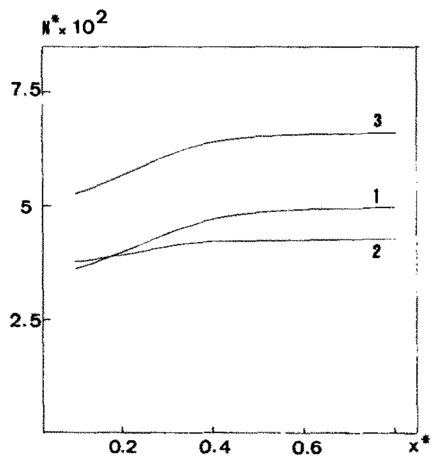

FIG. 16. Effect of the incident wall heat flux Q and the initial moisture content on the ratio N^*. 1, $w_p = 5$ kg kg^{-1} (dry basis), $Q = 500$ W m^{-2}; 2, $w_p = 5$ kg kg^{-1} (dry basis), $Q = 1000$ W m^{-2}; 3, $w_p = 3$ kg kg^{-1} (dry basis), $Q = 500$ W m^{-2}; $t = 1$ h; $\varepsilon = 0.5$; $\theta_\infty = 25°$C; $h_r = 5\%$; $\alpha = 0°$.

5. EXPERIMENTAL INVESTIGATION OF THE BOUNDARY LAYER

In order to give some quantitative validation of the above theory, the interferometric holography technique has been used for the experimental investigation of heat and mass transfer in the boundary layer. The details of this real-time method have been reported elsewhere [20, 21] and will not be repeated here.

The experimental sample is a parallelepipedic saturated pine wood plate ($0.3 \times 0.15 \times 0.02$ m), the heating of which is assured by four 150 W lights. The incident radiative heat flux was measured with a solarimeter whereas the plate temperature was controlled with two rows of thermocouples.

Figure 17 presents a typical interferogram and the two interesting geometrical parameters for the calculation of the local Nusselt and Sherwood numbers at point M: the distance AB from the wall and the distance x. For the special case of water vapour, the Schmidt number (0.68) and the Prandtl number (0.71) are very close, so that it is impossible to separate the interface fringes generated by concentration differences from those which have a thermal origin.

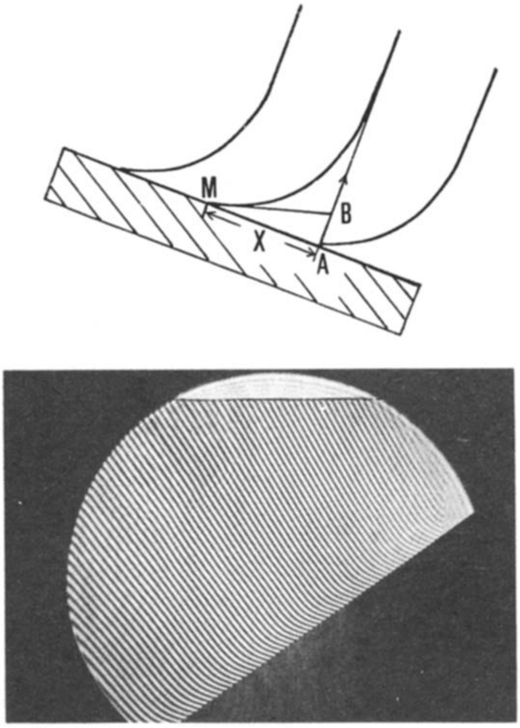

FIG. 17. Typical interferogram and definition of geometrical parameters used for the calculation of the local Nusselt and Sherwood numbers.

However, if $Pr = Sc$ is postulated, it can easily be shown that [21]

$$Nu_x = Sh_x = \frac{x}{\mathrm{AB}}. \tag{42}$$

The above equation only being valid for superficial evaporation. For internal evaporation, the Sherwood number is highly affected by the vapour diffusion in the porous material, which leads to smaller values of the mass transfer coefficient, as seen in the numerical results of this study. While experiments were carried out with a saturated porous material, Fig. 18 exhibits a reasonable agreement between theory and experimental data.

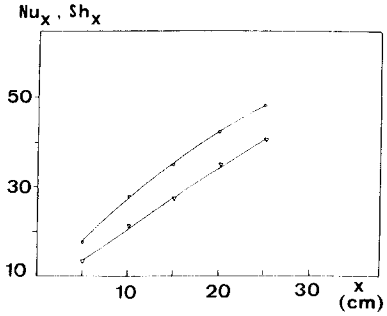

FIG. 18. Comparison between theoretical and experimental local Nusselt and Sherwood numbers at $x^* = 1$: $\alpha = 40°$; $\theta_r = 26°C$; $h_r = 38\%$; $Q = 460$ W m^{-2}.

6. CONCLUSION

A theoretical analysis of the transient free convection over an inclined wet flat plate has been presented. The problem is treated by linking the boundary-layer equations with the 'Luikov De Vries' model, the linkage conditions being assured by the wall heat and mass transfer balances. When the inclination angle from the vertical direction increases, it is found that the boundary-layer heat and mass transfer diminishes, so that the moisture removed from the plate also decreases. The average Nusselt and Sherwood numbers are first time decreasing before equating to their steady-state value. It has been shown that these values are highly affected by the internal vapour diffusion, so that the moisture removed is controlled by the structure of the porous material. For the special case of superficial evaporation, measurements with an interferometric holography method were carried out and comparison between theory and data shows a reasonably good agreement.

REFERENCES

1. E. V. Somers, Theoretical considerations of combined thermal and mass transfer from a vertical flat plate, *J. Appl. Mech.* **23,** 295–301 (1956).
2. W. G. Mathers, A. J. Madden and E. L. Piret, Simultaneous heat and mass transfer in free convection, *Ind. Engng Chem.* **49,** 961–968 (1957).
3. W. R. Wilcox, Simultaneous heat and mass transfer in free convection, *Chem. Engng Sci.* **13,** 113–119 (1961).
4. D. A. Saville and S. W. Churchill, Simultaneous heat and mass transfer in free convection boundary layers, *A.I.Ch.E. Jl* **16,** 268–273 (1970).
5. B. Gebhart and L. Pera, The nature of vertical natural convection flows resulting from the combined buoyancy effects of thermal and mass diffusion, *Int. J. Heat Mass Transfer* **4,** 2025–2049 (1971).
6. F. A. Bottemane, Theoretical solution of simultaneous heat and mass transfer by free convection about a vertical flat plate, *Appl. Scient. Res.* **25,** 137–149 (1971).
7. E. M. Sparrow and J. L. Cregg, Laminar free convection from a vertical plate with uniform surface heat flux, *J. Heat Transfer* **78,** 435–440 (1956).
8. M. Vachon, Etude de l'évaporation en convection naturelle, Thèse de docteur ingénieur, Poitiers (1979).
9. G. S. Callahan and W. J. Marner, Transient free convection with mass transfer on an isothermal vertical flat plate, *Int. J. Heat Mass Transfer* **19,** 165–174 (1976).
10. Y. Jaluria, *Natural Convection, Heat and Mass Transfer*. Pergamon Press, Oxford (1980).
11. R. Cheesewright, Natural convection from a plane vertical surface in non-isothermal surroundings, *Int. J. Heat Mass Transfer* **10,** 1847–1859 (1967).
12. B. R. Rich, An investigation of heat transfer from an inclined flat plate in free convection, *Trans. Am. Soc. Mech. Engrs* **75,** 489–499 (1953).
13. A. V. Luikov, *Heat and Mass Transfer in Capillary-porous Bodies*. Pergamon Press, Oxford (1966).
14. J. F. Sacadura, *Initiation aux transferts thermiques*. CAST, INSA de Lyon, TEC & DOC, Lavoisier (1978).
15. H. Chesseron, Contribution à l'étude du séchage solaire du bois, Thesis, Perpignan (1982).
16. W. T. Simpson, Predicting equilibrium moisture content of wood by mathematical models, *Wood Fiber* **1,** 41–49 (1973).

17. E. F. Nogotov, *Applications of Numerical Heat Transfer*. McGraw-Hill, New York (1978).
18. B. Carnahan, H. A. Luther and J. O. Wilkes, *Applied Numerical Methods*. Wiley, New York (1969).
19. R. Giblin, *Transmission de la chaleur par convection naturelle*, Collection de l'A.N.R.T. Eyrolles, Paris (1974).
20. S. Charar, S. Benet, S. Brunet, C. Delseny and R. Berge, Determination of the convection heat transfer coefficients of a solar-collector by holographic interferometry (NDT), Solar World Forum, Brighton (1981).
21. B. Zeghmati, Couplage entre les équations de Luikov et celles de la couche laminaire en convection naturelle au dessus d'une plaque inclinée, Thesis, Perpignan (1988).

ETUDE DE LA CONVECTION NATURELLE TRANSITOIRE SUR UNE PLAQUE PLANE HUMIDE ET INCLINEE

Résumé—On présente une analyse nouvelle de la convection naturelle transitoire entre une plaque humide et inclinée et l'air ambiant. Dans chacune des deux régions qu'il est possible de définir dans ce problème—à savoir la couche limite et la plaque poreuse—on écrit un système d'équations différentielles décrivant les transferts de masse et de chaleur. Les deux systèmes sont couplés à l'aide des bilans thermique et massique pariétaux, desquels on déduit les nombres de Nusselt et de Sherwood locaux et moyens. Les résultats théoriques s'accordent avec ceux préalablement publiés dans la littérature, pour quelques cas particuliers. Ces résultats sont aussi validés par une étude expérimentale de la couche limite.

UNTERSUCHUNG DER INSTATIONÄREN LAMINAREN FREIEN KONVEKTION AN EINER GENEIGTEN FEUCHTEN EBENEN PLATTE

Zusammenfassung—Eine neue analytische Untersuchung der instationären natürlichen Konvektion zwischen einer geneigten feuchten ebenen Platte und der umgebenden Luft wird vorgestellt. Zwei unterschiedliche Gebiete werden betrachtet: Die Grenzschicht und die kapillarporöse Platte. Dafür wird ein System von Differentialgleichungen formuliert. Die beiden Systeme sind durch die Wärmestromdichte und die Massenstromdichte an der Wandoberfläche gekoppelt, hieraus werden örtliche und mittlere Nusselt- und Sherwood-Zahlen abgeleitet. Für einige Sonderfälle werden die Ergebnisse mit Angaben aus früheren Arbeiten in der Literatur verglichen, wobei sich gute Übereinstimmung zeigt. Darüberhinaus ist die Übereinstimmung zwischen theoretischen Ergebnissen und Versuchsdaten im Grenzschichtgebiet befriedigend.

ИССЛЕДОВАНИЕ НЕСТАЦИОНАРНОЙ ЛАМИНАРНОЙ СВОБОДНОЙ КОНВЕКЦИИ НАД НАКЛОННОЙ ВЛАЖНОЙ ПЛОСКОЙ ПЛАСТИНОЙ

Аннотация—Проведен анализ нестационарной естественной конвекции над наклонной влажной плоской пластиной в окружающем воздухе. Для решения задачи исследуются раздельно две области: пограничный слой и капиллярно-пористая пластина—для каждой из них получены системы дифференциальных уравнений. Обе системы связаны балансом тепла и массы на стенке, из которого выводятся локальные и средние числа Нуссельта и Шервуда. Для некоторых случаев качественное сравнение показало их соответствие с результатами ранее опубликованных работ. Кроме того, получено удовлетворительное согласие между теоретическими результатами и экспериментальными данными для области пограничного слоя.